1521-0111/100/4/356–371$35.00
MOLECULAR PHARMACOLOGY

https://doi.org/10.1124/molpharm.121.000304
Mol Pharmacol 100:356–371, September 2021

ADP Ribosylation Factor 6 Promotes Contraction and Proliferation, Suppresses Apoptosis and Is Specifically Inhibited by NAV2729 in Prostate Stromal Cells

Ruixiao Wang, Stephanie Schneider, Oliver T. Keppler, Bingsheng Li, Beata Rutz, Anna Ciotkowska, Christian G. Stief, and Martin Hennenberg

Department of Urology, University Hospital Munich, LMU Munich, Munich, Germany (R.W., B.L., B.R., A.C., C.G.S., M.H.); and Max von Pettenkofer Institute and Gene Center, Virology, National Reference Center for Retroviruses, Faculty of Medicine, LMU Munich, Munich, Germany (S.S., O.T.K.)

Received April 4, 2021; accepted July 30, 2021

ABSTRACT

The presumed ADP ribosylation factor (ARF) 6 inhibitor NAV2729 inhibits human prostate smooth muscle contraction and proliferation of stromal cells, which are driving factors of voiding symptoms in benign prostatic hyperplasia (BPH). However, its specificity and a confirmed role of ARF6 for smooth muscle contraction are still pending. Here, we generated monoclonal ARF6 knockouts in human prostate stromal cells (WPMY-1), and characterized phenotypes of contractility, growth-related functions, and susceptibility to NAV2729 in knockout and control clones. ARF6 knockout was verified by Western blot. Knockout clones showed impaired contraction and actin organization, reduced proliferation and viability, and increased apoptosis and cell death. In ARF6-expressing control clones, NAV2729 (5 μM) strongly inhibited contraction (67% inhibition across all three control clones), actin organization (72%), proliferation (97%), and viability (up to 82%), and increased apoptosis (5-fold) and cell death (6-fold). In ARF6 knockouts, effects of NAV2729 (5 μM) were widely reduced, including lacking or minor effects on contractions (0% inhibition across all three knockout clones), actin (18%) and proliferation (13%), and lacking increases of apoptosis and cell death. Viability was reduced by NAV2729 with an IC_{50} of 3.3 μM across all three ARF6 control clones, but of 4.5–8.2 μM in ARF6 knockouts. In conclusion, ARF6 promotes prostate smooth muscle contraction and proliferation of stromal cells. Both are inhibited by NAV2729, which showed high specificity for ARF6 up to 5 μM and represents an attractive compound in the context of BPH. Considering the relevance of smooth muscle-based diseases, shared roles of ARF6 in other smooth muscle types merit further investigation.

SIGNIFICANCE STATEMENT

By knockout of ARF6 in prostate stromal cells, this study demonstrates the involvement of ARF6 in promotion of prostate smooth muscle contraction and stromal growth, and defines concentration ranges for their ARF6-specific inhibition by NAV2729. Besides the context of benign prostatic hyperplasia and lower urinary tract symptoms, analog ARF6 functions in contraction and growth appear possible in other smooth muscle-rich organs, which merits further attention considering the high clinical relevance of smooth muscle-based diseases.

Introduction

ADP ribosylation factor 6 (ARF6) belongs to the superfamily of monomeric GTPases. Major functions of ARF6 include cytoskeletal organization and actin remodeling, roles in endocytosis and vesicular trafficking, cell adhesion, and completion of mitotic cytokinesis in different cell types (Schafer et al., 2000; Donaldson, 2002; Luton, 2005; Schweitzer and D'Souza-Schorey, 2005; Klein et al., 2006; D'Souza-Schorey and Chavrier, 2006; Humphreys et al., 2013; Hongu and Kanaho, 2014). Accordingly, it promotes processes based on actin assembly and cytoskeletal organization, including migration, branching and outgrowth in neuronal cells, filopodia extension, platelet-mediated clot formation and thrombosis, or tumor angiogenesis and metastasis (Gauthier-Campbell et al., 2004; Choi et al., 2005; Hiroi et al., 2006; Torii et al., 2010; Charles et al., 2016; Hongu et al., 2016; Miura et al., 2016; Urban et al., 2016). With NAV2729, a small molecule inhibitor with presumed specificity for ARF6 is available (Yoo et al., 2016; Yamauchi et al., 2017). Recently, inhibition of prostate smooth muscle contraction, and of proliferation of prostate stromal cells by NAV2729, have been reported (Yu et al., 2019). ARF6-mediated promotion of smooth muscle contraction and proliferation appears

This work was supported by the Deutsche Forschungsgemeinschaft [Grant HE 5825/8-1]; and the Chinese Scholarship Council (CSC) [Grant 201608210185] (R.W.) and [Grant 201706370083] (B.L.).
https://doi.org/10.1124/molpharm.121.000304.

ABBREVIATIONS: 7-AAD, 7-aminoactinomycin D; ARF, ADP ribosylation factor; BPH, benign prostatic hyperplasia; CCK, cell counting kit; Ct, number of cycles; DAPI, 4′, 6-diamidino-2-phenylindole; EdU, 5-ethynyl-2′-deoxyuridine; FCS, fetal calf serum; GAPDH, glyceraldehyde-3-phosphate dehydrogenase; GEF, guanosine exchange factor; gRNA, guide RNA; LUTS, lower urinary tract symptom; NAV2729, 3-(4-chlorophenyl)-5-(4-nitrophenyl)-2-(phenylmethyl)pyrazolo[1, 5-a]pyrimidin-7(4H)-one; OD, optical density; PBS-T, PBS containing 0.1% Tween 20; RT-PCR, real-time polymerase chain reaction.

in fact plausible, considering that both processes are actin-dependent (Puetz et al., 2009; Jones et al., 2019; Hennenberg et al., 2014). However, the specificity of NAV2729 has been rarely examined, and a possible role of ARF6 in smooth muscle contraction or the involvement of ARF6 in NAV2729-mediated effects in prostate cells have not yet been confirmed using knockout models.

Previously reported effects of NAV2729 on prostate smooth muscle contraction and growth of stromal cells were discussed in the context of lower urinary tract symptoms (LUTSs) suggestive of benign prostatic hyperplasia (BPH). In BPH, increased prostate smooth muscle tone and prostate growth may cause urethral obstruction, resulting in impairments of urinary flow and bladder emptying, and finally in BPH-related voiding symptoms (Oelke et al., 2013; Hennenberg et al., 2014). Options for medical treatment include α_1-adrenoceptor antagonists, the phosphodiesterase-5 inhibitor tadalafil, and 5α-reductase inhibitors, which may improve symptoms or prevent progression of BPH and reduce the risk for complications and surgery (Oelke et al., 2013). Proposed mechanisms include prostate smooth muscle relaxation by α_1-adrenoceptor antagonists and tadalafil as well as inhibition of prostate growth by 5α-reductase inhibitors (Oelke et al., 2013). Considering that their overall efficacy is insufficient, together with the high and age-dependent prevalence of LUTS suggestive of BPH and the demographic transition, alternative options for medical treatment are of high demand, requiring identification of new targets and novel candidate compounds. Currently, separate medications are needed to target prostate smooth muscle contraction and growth. Connections between both processes have been merely considered in the past, although both may contribute to LUTS suggestive of BPH.

Consequently, identifying molecular mechanisms linking smooth muscle contraction with stromal growth in the prostate provides new concepts in understanding of BPH and may offer attractive targets for putative medical interventions against BPH in the future (Hennenberg et al., 2014). Findings obtained by application of NAV2729 to prostate tissues allow to assume such a dual role of ARF6 in proliferation and contraction of prostate smooth muscle cells, which needs, however, to be confirmed (Yu et al., 2019). A similar function has been attributed to the monomeric GTPase RhoA. RhoA-mediated contraction and proliferation of smooth muscle cells has been confirmed for all types of smooth muscle and is widely accepted (Somlyo and Somlyo, 2003). Similar roles of other monomeric GTPases in smooth muscle contraction of different smooth muscle-rich organs are an emerging field (Li et al., 2020a). Considering that widespread diseases including arterial hypertension or obstructive airway diseases are related to aberrant smooth muscle contraction, proving a role of ARF6 in smooth muscle contraction may be of interest even beyond BPH and LUTS. Here, we created ARF6 knockout clones of human prostate stromal cells to 1) confirm a role of ARF6 in smooth muscle contraction and proliferation and 2) to characterize the specificity of NAV2729.

Materials and Methods

Cell Culture. WPMY-1 cells are a simian virus 40 (SV40) large-T antigen-immortalized cell line, obtained from the stroma of a human prostate without prostate cancer (Webber et al., 1999). It is reported that this cell line is hyperdiploid, X–Y, with chromosome numbers varying from 58 to 68 (Webber et al., 1999). According to the typical composition of the prostate stroma, where smooth muscle cells are the predominant cell type, WPMY-1 cells show characteristics of myofibroblasts and prostate smooth muscle cells, including expression of vimentin, α-smooth muscle actin, calponin, and α_{1A}-adrenoceptors, but lack expression of cytokeratins and tyrosine hydroxylase (Webber et al., 1999; Wang et al., 2015; Wang et al., 2016). Here, polyclonal, parental WPMY-1 cells were used to create ARF6 knockout clones and corresponding controls with ARF6 expression. WPMY-1 cells were purchased from the American Type Culture Collection (Manassas, VA), and cultured in RPMI 1640 (Gibco, Carlsbad, CA) supplemented with 10% fetal calf serum (FCS) and 1% penicillin/streptomycin at 37°C with 5% CO_2. Before addition of NAV2729 or DMSO (solvent for NAV2729) to parental WPMY-1 cells, ARF6 knockout clones, or ARF6 control clones, the medium was changed to an FCS-free medium.

Vectors and Transfection. pLKO.1 cytomegalovirus (CMV) gRNA ARF6 GFP mammalian expression plasmid that contains gRNA for knockout generation in ARF6 gene, and pRZ blue fluorescent protein (BFP) thosea asigna virus 2A self cleaving peptide (T2A) clustered regularly interspaced short palindromic repeats associated protein 9 (Cas9) mammalian expression plasmid that contains Cas9 for knockout generation were kindly provided by Veit Hornung, Gene Center, LMU Munich, Germany. The target site for ARF6 gRNA in the ARF6 gene was 5′-TGGGAATGGTGGTCACCGACTGG-3′. The two plasmids were cotransfected (1:1 ratio) into WPMY-1 cells using human prostate stromal cell avalanche transfection reagent (EZ Biosystems, College Park, MD). For transfection, WPMY-1 cells were plated into 6-well plates, grown to 70% confluency, and cultured without antibiotics 24 hours prior to transfection. Transfection mix for each well contained the two plasmids (4 μg of each plasmid) and 5 μl transfection reagent in 200 μl of Opti-MEM (Gibco), which were merged and incubated at room temperature 15 minutes before addition to wells. After dropwise addition of the transfection mixture into wells, plates were centrifuged (300 *g*, 5 minutes) and subsequently incubated for 5 hours (37°C, 5% CO_2) before the medium was replaced by normal, antibiotic-containing RPMI. Successful transfections of plasmids were visually verified under a fluorescent microscope using channels for fluoresceine isothiocyanate and 4′,6-diamidino-2-phenylindole (DAPI). Subsequently, successfully double-transfected cells were separated and isolated by cell sorting using a BD FACSMelody Cell Sorter (BD Biosciences, San Jose, CA) at the Flow Cytometry Facility, Gene Center, LMU Munich, Germany.

Single Cell Dilution and Sequencing. After cell sorting, cells were diluted in RPMI medium to obtain a final dilution between 0.5 and 1 cell/well. Resulting aliquots were seeded into 96-well plates (100 μl/well) and cultured for 4 weeks (37°C, 5% CO_2). Successfully growing clones were sequenced using a MiSeq benchtop sequencing system (Illumina, San Diego, CA) (Schmid-Burgk et al., 2014). After sequencing, the following clones were selected for further experiments: three ARF6 knockout clones (monoclonal, heterogenous ARF6 knockout clones), in which three alleles were detected via deep sequencing and 1 out of 3 alleles (referred to as knockout clone C4) or 2 out of 3 alleles (knockout clones B4 and B9) showed an out-of-frame mutation at the site of editing, and three ARF6 control clones. Monoclonal ARF6 control clones went through the whole procedure as the knockout clones but do not show any edited sequence in the region where the gRNA for ARF6 was binding (referred to as control clones A3, C6, and D7). ARF6 knockout and control clones were verified by Western blot, as described below.

Western Blot Analysis. Cells were prepared in T75 flasks, and protein isolation was performed when cells reached 80% confluency. For protein isolation, cells were washed twice with ice-cold PBS. Subsequently, 600 μl of radioimmunoprecipitation assay buffer (Sigma-Aldrich, Munich, Germany) containing 5 μl protease inhibitor cocktail (P8340, Sigma-Aldrich) were added to each flask. After incubation on ice for 25 minutes, lysed cells were removed from flasks, and cell debris was removed by centrifugation (10,000 *g*, 10 minutes, 4°C). Protein concentrations were determined using aliquots of 40 μl of each sample and a protein quantification assay (catalog number 740967,

Macherey-Nagel, Düren, Germany) according to the manufacturer's instructions. Remaining samples were boiled for 10 minutes with SDS sample buffer (Roth, Karlsruhe, Germany). Samples were subjected to SDS polyacrylamide gel electrophoresis (20 μg/lane), and proteins were blotted on Protran nitrocellulose membranes (Schleicher and Schuell, Dassel, Germany). For blockage of unspecific binding sites, membranes were blocked with PBS containing 5% milk powder (Roth, Karlsruhe, Germany) over night. Subsequently, membranes were washed three times (each time for 5 minutes) with PBS containing 0.1% Tween 20 (PBS-T), followed by incubation with mouse monoclonal anti-ARF6 (sc-7971) antibody or mouse monoclonal anti–β-actin antibody (sc-47778) (all from Santa Cruz Biotechnology, Santa Cruz, CA) for 90 minutes. Primary antibodies were diluted 1:200 (ARF6 antibody) or 1:800 (β-actin antibody) in PBS-T containing 5% milk powder. Thereafter, membranes were again washed with PBS-T (four times, each time for 5 minutes) followed by incubation with secondary biotinylated horse anti-mouse IgG (BA-2000) (Vector Laboratories, Burlingame, CA) (diluted 1:1,500 in PBS-T containing 5% milk powder), washed again with PBS-T (four times, each time for 5 minutes), incubated with avidin and biotinylated horseradish peroxidase from the Vectastain ABC kit (Vector Laboratories, Burlingame, CA) both diluted 1:200 in PBS, and washed again with PBS-T (four times, each time for 5 minutes). Finally, blots were developed with enhanced chemiluminescence using ECL Hyperfilm (GE Healthcare, Freiburg, Germany). Intensities of presumed ARF6 bands and bands for β-actin were quantified densitometrically using Image J (National Institutes of Health, Bethesda, Maryland) and referred to β-actin in corresponding samples.

Contraction Assay. Contractility of cells was measured using the Floating Matrix model version of the CytoSelect 24-Well Cell Contraction Assay Kit (Cell Biolabs, San Diego, CA). Cells were cultured in T75 flasks for 72 hours before being trypsinized and resuspended in fresh RPMI medium to a dilution 5×10^6 cells/ml. Each well of the 24-well plates provided with the kit was filled with a matrix plug containing 100 μl of the trypsinized cell suspension and 400 μl of collagen gel working solution provided with the kit, which was mixed before filling to the wells. After incubation for 1 hour (37°C, 5% CO_2) and collagen polymerization during this incubation, 1 ml RPMI medium (containing either no NAV2729 or DMSO, or NAV2729 as indicated or DMSO in corresponding amounts) were added, and incubation was continued (37°C, 5% CO_2). For monitoring of collagen contraction, pictures were taken 1 hour and 3 hours after adding of RPMI (corresponding to 2 hours and 4 hours after trypsinization). Diameters and areas of the collagen plugs and wells on pictures were quantified using Image J, resulting in values for 1) changes of the plug diameter (in mm; Δ of whole well diameter and of plug diameter at indicated time points) and 2) ratios between the collagen-covered area and the area of the whole well. Both quantification methods have been recommended by the manufacturer, and were applied here for quantification of the same experiments.

Phalloidin Staining. For comparisons of proliferation rates between cell lines, 10,000 cells of each line were placed in each well of a 16-well chambered coverslip (Thermo Scientific, Waltham, MA) and cultured in FCS-free medium. Cells were fixed with ROTI Histofix 4% solution (Roth, Karlsruhe, Germany) after 72 hours of culture, and staining with 100 μM fluoresceine isothiocyanate–labeled phalloidin (Sigma-Aldrich, Munich, Germany) was performed in each well according to the manufacturer's instruction. Labeled cells were analyzed using a laser scanning microscope (Leica SP2, Wetzlar, Germany). Finally, all stainings were quantified using Image J (National Institutes of Health, Bethesda, Maryland). To assess effects of NAV2729, again 10,000 cells were placed in each well of 16-well chambered coverslips, and incubated 24 hours. Subsequently, NAV2729 or DMSO were added as indicated, followed by incubation for further 24 hours without or with NAV2729 or DMSO. Finally, cells were fixed, stained, and analyzed as described above.

Proliferation Assay. Proliferation rate of cells was assessed using the 5-ethynyl-2′-deoxyuridine (EdU)-based EdU-Click 555 proliferation assay kit (Baseclick, Tutzing, Germany), which was applied according to the manufacturer's instructions. In this assay, incorporation of EdU into DNA of proliferating cells is assessed by detection with fluorescing 5-carboxytetramethylrhodamine. For comparisons of proliferation rates between cell lines, 10,000 cells of each line were placed in each well of a 16-well chambered coverslip (Thermo Scientific, Waltham, MA) and cultured in FCS-free medium. EdU was added after 48 hours as a 10 mM stock solution. 24 hours later, cells were fixed with ROTI Histofix 4% solution (Roth, Karlsruhe, Germany). Counterstaining of all nuclei was performed with DAPI. Finally, analysis was performed by fluorescence microscopy (excitation: 546 nm; emission: 479 nm) using a laser scanning microscope (Leica SP2, Wetzlar, Germany). Stainings were quantified using Image J (National Institutes of Health, Bethesda, Maryland). To assess effects of NAV2729, again 10,000 cells were placed in each well of 16-well chambered coverslips and cultured for 24 hours in FCS-free medium before NAV2729 in indicated concentrations or DMSO in required amounts were added. After incubation for further 24 hours, the medium was replaced by 10 mM EdU solution in FCS-free smooth muscle cell medium containing NAV2729 or DMSO.

Assessment of Ki-67 Content. As an indicator of proliferation, Ki-67 mRNA content of cells was semiquantitatively assessed by RT-PCR. Compared with resting cells [G(0) phase], Ki-67 is upregulated during all active phases of the cell cycle and of mitosis (Scholzen and Gerdes, 2000). Consequently, it is a suitable marker for proliferation and has been commonly assessed to monitor proliferation in various cell types, including airway and vascular smooth muscle cells or WPMY-1 cells (Halwani et al., 2013; Dai et al., 2019; Yu et al., 2019). Cells were seeded in 6-well plates and grown to 70% confluency. Subsequently, NAV2729 or DMSO were added as indicated, 24 hours before RNA isolation. RNA isolation and RT-PCR were performed as described below.

RT-PCR. RNA from cells was isolated by using the RNeasy Mini kit (Qiagen, Hilden, Germany) according to the manufacturer's instructions. RNA concentrations were measured spectrophotometrically. Reverse transcription to cDNA was performed with 1 μg of isolated RNA using the reverse transcription kit (Promega, Madison, WI). Ki-67 and glyceraldehyde 3-phosphate dehydrogenase (GAPDH) mRNA was detected using a Roche Light Cycler (Roche, Basel, Switzerland). Ready-to-use primers were purchased from Qiagen (Hilden, Germany) based on the RefSeq accession numbers NM_001145966 for Ki-67 and NM_002046 for GAPDH. Polymerase chain reactions were performed in a volume of 25 μl containing 5 μl LightCycler FastStart DNA MasterPlus SYBR Green I (Roche, Basel, Switzerland), 1 μl template, 1 μl primer, and 18 μl water. Denaturation was performed for 10 minutes at 95°C, and amplification with 45 cycles of 15 seconds at 95°C followed by 60 seconds at 60°C. The specificity of primers and amplification was demonstrated by subsequent analysis of melting points, which revealed single peaks for each target. Results were expressed using the ΔΔCt method, where number of cycles (Ct) at which the fluorescence signal exceeded a defined threshold for GAPDH was subtracted from Ct values for Ki-67 ($Ct_{Ki\text{-}67}$-Ct_{GAPDH} = ΔCt), and values were calculated as $2^{-\Delta Ct}$ and normalized to the mean values of corresponding controls.

Cell Apoptosis Analysis. A flow cytometry–based annexin V allophycocyanin and 7-aminoactinomycin D (7-AAD) apoptosis detection kit (BD Biosciences, Franklin Lakes, NJ) was used to detect apoptotic (annexin V–positive, 7-AAD–negative) and dead (annexin V–positive, 7-AAD–positive) cells. Cell death in annexin V–positive/7-AAD–positive cells may result from apoptosis or necrosis, which cannot distinguished by this assay. For comparisons between cell lines, around 100,000 cells were seeded in 6-well plates. After 48 hours, cells were washed with PBS and resuspended in annexin V binding buffer (BD Biosciences) followed by addition of 5 μl allophycocyanin annexin V and 5 μl 7-AAD reagent to each sample. After incubation in the dark for 15 minutes at room temperature, 400 μl binding buffer was added to each sample before analysis by flow cytometry. To assess effects of NAV2729, the procedure was the

same, but NAV2729 or DMSO were added 24 hours after seeding into 6-well plates (24 hours before washing with PBS).

Viability Assay. Viability was assessed using the Cell Counting Kit-8 (CCK-8) (Sigma-Aldrich, Munich, Germany). Cells were seeded in 96-well plates (5000 cells/well) and cultured for 48 hours, 72 hours, or 96 hours. Finally, 10 μl of 2-(2-methoxy-4-nitrophenyl)- 3-(4-nitrophenyl)-5-(2,4-disulfophenyl)-2H-tetrazolium monosodium salt from the kit were added, and absorbance in each well was measured at 450 nm after incubation for 2 hours at 37°C. To assess effects of NAV2729, again 5,000 cells/well were seeded in 96-well plates and cultured for 24 hours. Subsequently, NAV2729 in indicated concentrations or DMSO in required amounts were added, and cells were cultured for further 24 hours until assessment. IC_{50} values for NAV2729 were calculated by curve fitting using GraphPad Prism 6 (Statcon, Witzenhausen, Germany) and analyzed as described below, based on experiments including a concentration range of 1.25 μM to 15 μM. For curve fitting, OD values were normalized to the DMSO control (set to 100%), which was not included in curve but set as maximum y value, as variations of non-normalized, maximum OD values impeded plausible results from curve fitting. Automatic curve fitting was performed separately for each single experiment to obtain single values for each single experiment. Sigmoidal concentration response curves were fitted by nonlinear regression, without predefined constraints for bottom, top, or IC_{50} values, by ordinary fit, without weighting, and without choosing automatic outlier elimination.

Drugs and Nomenclature. NAV2729 (3-(4-Chlorophenyl)-5-(4-nitrophenyl)-2-(phenylmethyl)pyrazolo[1,5-a]pyrimidin-7(4H)-one) is a small molecule inhibitor with assumed selectivity for ARF6, and was obtained from Tocris (Bristol, UK). The batch used here (2A/246293) was analyzed for quality control by the provider and showed a purity of 99% in high-performance liquid chromatography. ^1H nuclear magnetic resonance spectroscopy and mass spectrometry were both consistent with the structure, and contents of carbon, hydrogen, and nitrogen found in microanalyses were consistent with theoretical values (carbon theoretical/found 65.72/65.65, hydrogen 3.75/3.69, nitrogen 12.26/12.24). The structure of NAV2729 has been made available in PubChem (PubChem ID 2257249), and in the supplementary material of a recent article (Benabdi et al., 2017). NAV2729 inhibits ARF6 by direct binding to ARF6 and preventing its activation by guanosine exchange factors (GEFs), as well as its spontaneous activation occurring partially without nucleotide binding to ARF6 (Yoo et al., 2016; Yamauchi et al., 2017). Consequently, ARF6 inhibition does not depend on the identity of GEFs, which may vary between cell types (Hongu and Kanaho, 2014; Yamauchi et al., 2017). Stock solutions (10 mM) were prepared in DMSO and stored at −20°C until use.

Data and Statistical Analyses. Our study aimed to examine effects of 1) ARF6 knockout in human prostate stromal cells, and 2) of NAV2729 treatment on contraction and growth-related functions in human prostate stromal cells with ARF6 knockout, in corresponding control cells with ARF6 expression, and in the parental cell line, i.e. WPMY-1 cells. After creation and selection of knockout and control clones, contraction, actin organization, proliferation, apoptosis and cell death, and viability were compared between control cell lines and knockout clones, and effects of NAV2729 treatment on the same parameters were examined in all cell lines. After creation and selection of knockout and control clones as described above, each series of experiments was preplanned to include five independent experiments, what was abided in all series (except of Western blot analyses, for reasons described below). Despite this preset study design, criteria for a strict hypothesis-driven character are not met, for following reasons. Firstly, knockout and control clones were selected for further experiments after results from sequencing were obtained. Consequently, large parts of the study were adapted to these initial results, what is a clear feature excluding a hypothesis-testing character (Michel et al., 2020). Secondly, experiments were performed without blinding. Thirdly, definition of clear null hypotheses was not possible. Accordingly, and in line with recent guidelines for reporting data, data analysis, and statistical methods, our study should be considered as exploratory (Michel et al., 2020). No data were omitted, with the exception of Western blot analyses, for reasons explained below. Samples in Ki-67 analyses were determined in duplicate by RT-PCR, whereas all other quantifications and values are based on single samples and single determinations.

According to the exploratory character, reported P values are descriptive but not hypothesis-testing. In line with recent guidelines recommending sparing use of P values and to focus on effect sizes instead of P values (Michel et al., 2020), reporting of P values was limited to most relevant comparisons. Consequently, comparisons between cell lines did not include parental cells but were limited to knockout and control clones, and no comparisons were performed within the three control clones or within the three knockout clones. Again, to use P values sparingly and to maintain an appropriate degree of clearness in presentation, control clones were summarized to one group (i.e., a cluster containing all values from all three clones, 15 values in total) for statistical analyses, and values for each knockout clone were compared with this control group. Considering that low P values do not necessarily reflect large effect sizes (Michel et al., 2020), P values are here reported as symbols instead of exact or approximated values. Multiple comparisons between cell lines were performed by one-way ANOVA with Dunnett's tests, which allows comparison of a number of groups with a single control group. Comparisons in series including more than one concentration of NAV2729 and a control group (DMSO) in each single experiment were again performed by one-way ANOVA with a Dunnett's test. Comparisons in series including only one concentration of NAV2729 and a control group (DMSO) were performed by a two-tailed Student's t test, which allows comparison between two groups. All tests were performed using GraphPrism 6 (Statcon, Witzenhausen, Germany). Comparisons in experiments with DMSO and NAV2729 are based on paired samples, as each independent experiment included application of DMSO and NAV2729 (including all concentrations as indicated) to the same cell line in the same experiment. P values < 0.05 were considered significant.

All data are presented in scatter plots (instead of bar graphs or concentration response curves), including all single values and means together with images of representative experiments (if applicable) as recently recommended by guidelines for displaying data in experimental biology (Michel et al., 2020). As the focus of data presentation was on effect sizes and variabilities, exemplarily or relevant effect sizes in the text are reported as mean difference or as means of clone clusters (i.e., all three control clones and of knockout clones) with 95% confidence intervals, which were calculated using SPSS version 20 (IBM SPSS Statistics, IBM Corporation, Armonk, New York) and are presented in square brackets.

Western blot analyses were preplanned with a minimum number of seven experiments, as a minimum of $n = 5$ independent experiments was generally intended for each series, but we assumed in advance that 1) some samples may be too small to allow Western blot analysis (i.e. do not provide 2 x 20 μg, required for ARF6 and β-actin blots, in at least one sample of a series), 2) detection may fail in some samples, 3) blots may be unsuitable for quantification, e.g. due to artifacts, or 4) outliers may occur. Consequently, seven independent experiments were performed for Western blot analyses. In fact, 2) occurred in one experiment, where ARF6 bands in a control cell line remained too weak to allow conclusive densitometric quantification, and 3) occurred in another experiment, where streaks covered parts of the band areas, resulting in unclean blots and impeding conclusive densitometric quantification. Thus, although ARF6 bands in these blots showed the same pattern as the other blots, these experiments could not be included at all, and presented Western blot analyses are based on five of seven experiments. All samples from one series were analyzed in the same blot.

Results

ARF6 Knockout Generation in WPMY-1 Cells. From 104 sequenced single cell clones, six met the criteria for further experimentation, including three different ARF6-expressing control clones (in the following referred to as control A3, control C6 and control D7, or together as monoclonal ARF6 control clones), one clone showing ARF6 knockout in one of three alleles (referred to as single ARF6 knockout C4, or single ARF6 knockout clone), and two clones showing ARF6 knockout in two of three alleles (referred to as double knockout B4 or B9, or together as double knockout clones). Knockout of ARF6 in knockout clones was verified by Western blot analyses (Fig. 1).

Effects of NAV2729 and ARF6 Knockout on Cell Contraction. Cell contractions were assessed by matrix contraction assays. Compared with ARF6-expressing cell lines (WPMY-1 and three monoclonal ARF6 control clones), all three knockout clones showed reduced contractions, as reflected by reduced changes in diameters of collagen matrix plugs and by increased gel areas (the latter normalized to well areas, and expressed as ratios of gel area/matrix area) (Fig. 2A). Thus, within 1 hour after adding RPMI to assay wells, matrix plugs contracted by 1.51 mm [1.18 to 1.84] across all three ARF6-expressing control clones, but around 0.58 mm [0.2 to 0.96] in all three ARF6 knockout clones. Accordingly, average ratios between gel areas and well areas ranged around 0.83 [0.77 to 0.88] across all three ARF6-expressing control clones 1 hour after adding of RPMI, but around 0.94 [0.91 to 0.96] in all three ARF6 knockout clones. Within 3 hours after adding RPMI, matrix plugs contracted by 3.68 mm [3.56 to 3.8] across all three ARF6-expressing control clones, but around 2.43 mm [1.54 to 3.33] in all three ARF6 knockout clones. Accordingly, average ratios between gel areas and well areas ranged around 0.67 [0.6 to 0.74] across all three control clones 3 after adding RPMI, but around 0.77 [0.74 to 0.81] across all three knockout clones.

In the next series, effects of NAV2729 were assessed in all cell lines, by comparison of plug diameters and areas after addition of DMSO or NAV2729 (Fig. 2, B and C). In all four ARF6-expressing cell lines, the changes in plug diameter were lower, and gel area/well area ratios were larger in cells exposed to NAV2729 compared with cells exposed to DMSO, which was observed 1 hour and 3 hours after adding RPMI with DMSO or NAV2729 (5 μM) and reflects inhibition of contraction by NAV2729 (Fig. 2, B and C). Across all three ARF6-expressing control clones, matrix plugs contracted on average by 1.9 mm [1.32 to 2.47] within 1 hour after application of DMSO, but around 0.66 [0.21 to 1.11] within 1 hour after application of NAV2729. In contrast, matrix plugs contracted on average by 1.16 mm [0.11 to 2.22] within 1 hour after application of DMSO, and around 1.16 [0.52 to 1.8] within 1 hour after application of NAV2729 across all three knockout clones. Within 3 hours after application of DMSO

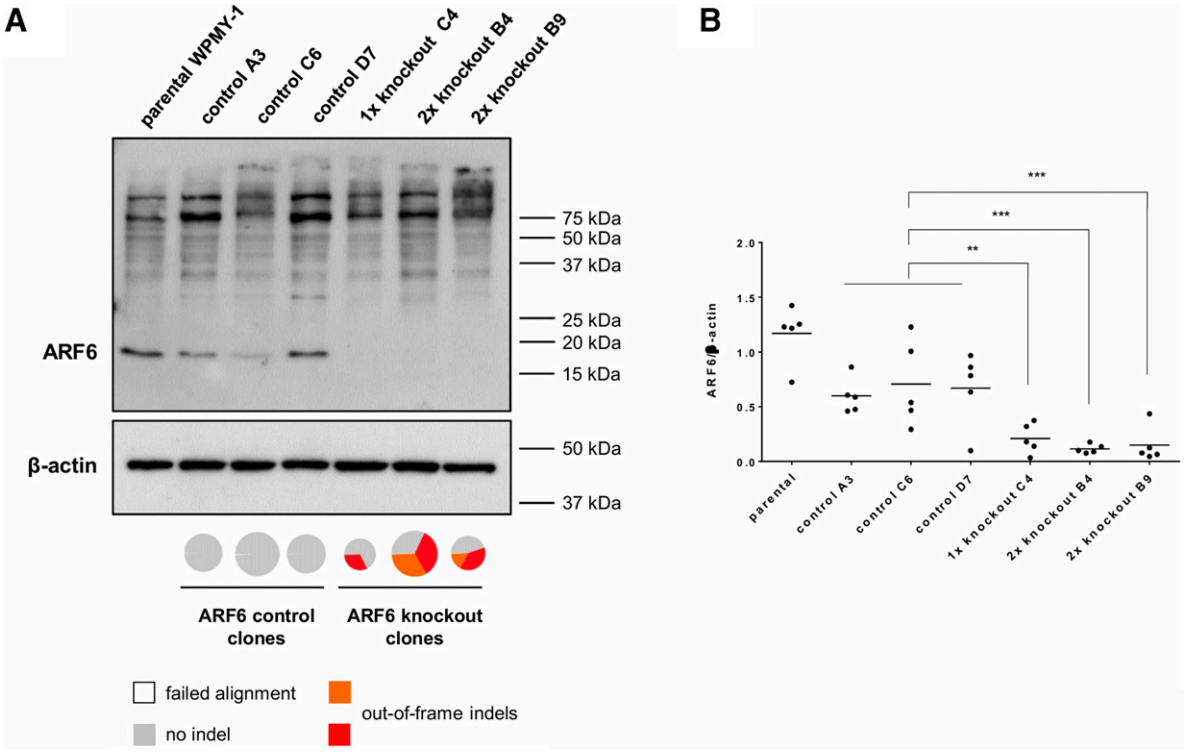

Fig. 1. ARF6 knockout in WPMY-1 cells. Western blot analyses of parental cells (WPMY-1), ARF6-expressing monoclonal control clones (controls A3, C6, D7), and monoclonal ARF6 knockout clones (single allele knockout clone C4, and double allele knockout clones B4 and B9) were performed using an antibody raised against ARF6 and β-actin. In (A), representative Western blots together with positions of a molecular weight marker indicating expected sizes of detected proteins and pie charts are shown. Pie charts represent the MiSeq analysis of clones on the DNA level as well as the verification of triploids in this particular cell line. Red and orange colors represent two different out-of-frame mutations at the site of editing. Gray pie charts mean that no indel (no change) was detected at the particular site of editing. The size of pie chart represents the number of reads in the sequencing and indicates that all clones showed sufficient sequencing reads. In (B), all single values (ratios of band intensities as indicated) of all samples obtained from quantification of five independent experiments are shown. Values of each knockout clone were compared with a cluster containing all values of all control clones by one-way ANOVA with Dunnett's tests (** $P < 0.01$, *** $P < 0.001$ versus a control group composed of all values of A3, C6 and D7). Parental WPMY-1 cells were not included to statistical analyses.

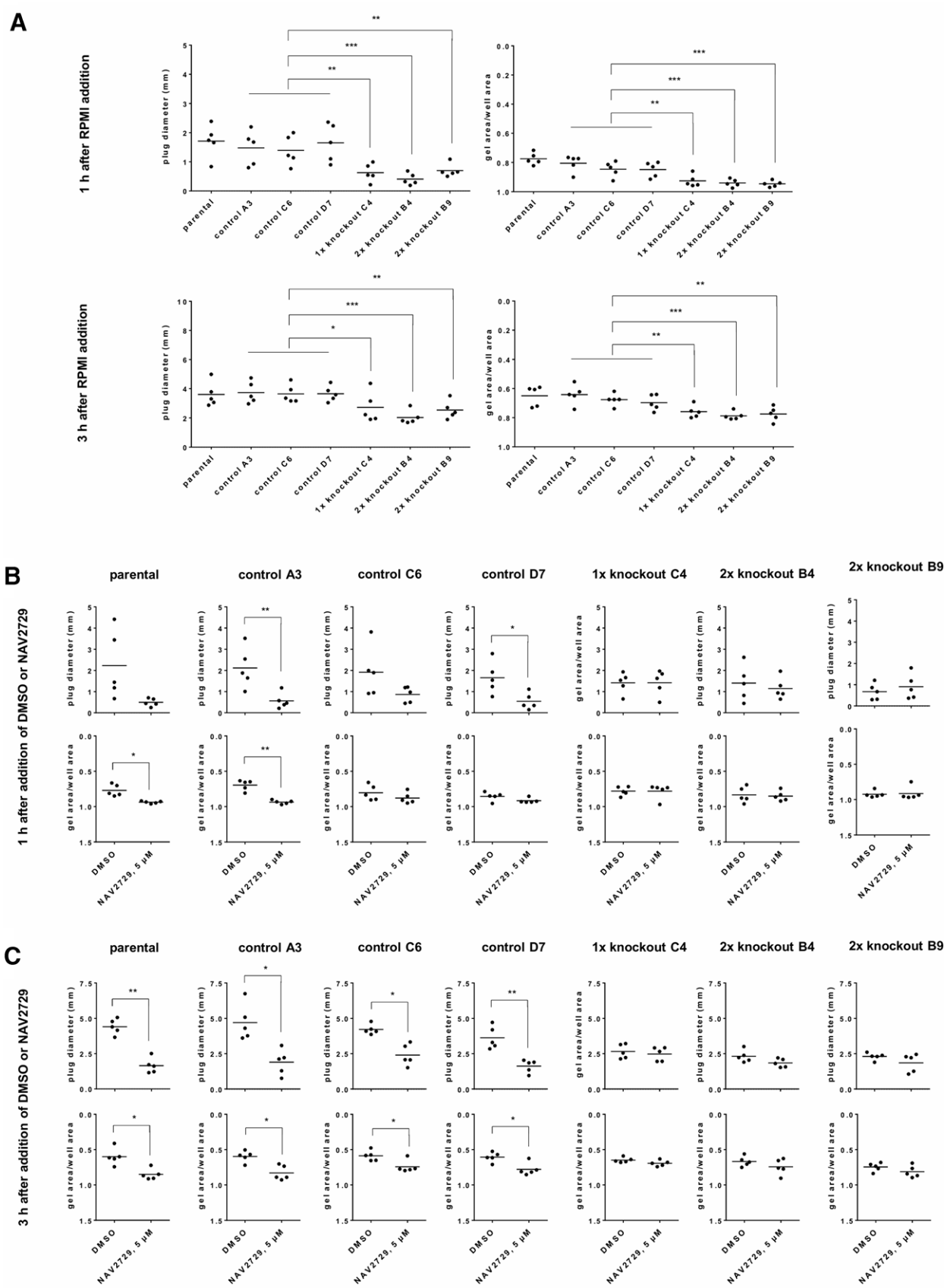

Fig. 2. Contraction of WPMY1 cells, ARF6 control clones, and ARF6 knockout clones. Contractions were compared between cell lines (A), and between cells exposed to DMSO or NAV2729 (5 μM) for 1 hour (B) or 3 hours (C). Cells were seeded in matrix plugs, without or with DMSO or NAV2729, and areas of plugs and whole wells were assessed after indicated periods after 1 hour or 3 hours after addition of RPMI with or without DMSO or NAV2729 to plugs. Separate series of experiments were performed to compare contraction between cell lines (A), and to assess

or NAV2729, matrix plugs contracted on average by 4.18 mm [2.84 to 5.52] after DMSO, but around 1.97 [0.99 to 2.96] after NAV2729 across all three ARF6-expressing control clones. In contrast, changes in diameters were again similar after application of DMSO and NAV2729 across all three knockout clones, averaging to 2.43 mm [1.93 to 2.92] within 3 hours after application of DMSO, and around 2.06 [1.15 to 2.97] within 3 hours after application of NAV2729.

Similar patterns were observed, if ratios between plug areas and well areas were calculated and compared between DMSO and NAV2729 groups (Fig. 2, A and B). Thus, average ratios between gel areas and well areas ranged around 0.78 [0.58 to 0.99] 1 hour after application of DMSO, but around 0.91 [0.84 to 0.98] 1 hour after application of NAV2729. 3 hours after application of DMSO, average ratios between gel areas and well areas ranged around 0.6 [0.57 to 0.62], but around 0.78 [0.67 to 0.89] 3 hours after application of NAV2729 across all three control clones. Six hours after application of DMSO, average ratios between gel areas and well areas ranged around 0.49 [0.44 to 0.55], but around 0.67 [0.48 to 0.86] 6 hours after application of NAV2729 across all three control clones. In all three knockout clones, effects of NAV2729 were widely reduced or lacking (Fig. 2B). Across all three ARF6 knockout clones, average ratios between gel areas and well areas ranged around 0.85 [0.66 to 1] 1 hour after application of DMSO, and around 0.85 [0.68 to 1] 1 hour after application of NAV2729. 3 hours after application of DMSO, average ratios between gel areas and well areas ranged around 0.69 [0.56 to 0.82], and around 0.75 [0.6 to 0.9] 3 hours after application of NAV2729 across all three knockout clones. 6 hours after application of DMSO, average ratios between gel areas and well areas ranged around 0.56 [0.49 to 0.63], and around 0.63 [0.51 to 0.76] 6 hour after application of NAV2729 across all three knockout clones.

Effects of NAV2729 and ARF6 Knockout on Actin Organization. Polymerized actin was visualized by phalloidin staining. In WPMY-1 cells and monoclonal ARF6 control clones, actin was organized to long filaments and bundles, showing parallel arrangement and forming elongated protrusions, with filaments from different cells overlapping each other after 72 hours of culture (Fig. 3A). Phalloidin-stained actin covered more than 50% of microscopic fields in these cells (Fig. 3A). This actin organization observed in parental cells and control clones was widely lost in all three ARF6 knockout clones (Fig. 3A). Remaining actin in knockout clones formed short and thicker filaments, or was arranged around the nucleus and just forming jag-like structures (Fig. 3A). In addition to these qualitative changes, the extent of actin-stained areas was lower compared with parental cells and control clones. Phalloidin-stained areas covered more than 50% of microscopic fields in all ARF6-expressing cell lines (mean 55% [49 to 61] for the three control clones), but less than 40% of microscopic fields in all three Arf6 knockout clones (36% [29 to 43]) (Fig. 3A).

In parental cells and ARF6 control clones, application of NAV2729 (2.5 μM, 5 μM) for 24 hours caused concentration-dependent breakdowns of actin organization and reduced the content of phalloidin-stained areas (Fig. 3B). At qualitative level, the breakdown of actin organization caused by NAV2729 was characterized by concentration-dependent loss of the drawn-out filament structure of stained actin (Fig. 3B). Compared with corresponding, DMSO-treated controls, remaining actin formed shorter and broader protrusions instead of clear filaments after exposure to 2.5 μM NAV2729, while no protrusions were formed, and actin was largely centered around nuclei after exposure to 5 μM NAV2729 (Fig. 3B). Quantitative changes resulting from NAV2729 were similar in all four cell lines, and included reductions of actin-covered areas around 40% by 2.5 μM NAV2729, and 70% by 5 μM NAV2729 (Fig. 3B). Across all three ARF6-expressing control clones, average actin-covered areas ranged around 53% [44 to 63] after application of DMSO, but around 33% [11 to 56] after application of 2.5 μM NAV2729 and around 15% [7 to 23] after application of 5 μM NAV2729 (Fig. 3B).

In contrast to parental WPMY-1 cells and control clones, NAV2729 was without effect on the remaining content of phalloidin-stained actin in single knockout clones and in both double allele knockout clones. At qualitative level, a loss of actin organization to filaments became obvious in solvent-treated knockout clones. Other than in DMSO-treated ARF6 knockout clones, actin did not form long and thin filaments. Remaining protrusions were short, forming jagged structures and resulting a star-like shape of cells. Similarly, remaining filaments in both double allele knockout clones did not form protrusions anymore, but rather jags or edges, giving the cells a triangular shape. At quantitative level, 2.5 μM NAV2729 remained without effect on phalloidin-stained areas, whereas 5 μM NAV2729 reduced the phalloidin-stained areas by approximately 17%. Across all three knockout clones, average actin-covered areas ranged around 45% [28 to 61] after application of DMSO, around 44% [26 to 61] after application of 2.5 μM NAV2729, and around 37% [23 to 51] after application of 5 μM NAV2729 (Fig. 3B).

Effects of NAV2729 and ARF6 Knockout on Proliferation. Proliferation was assessed by EdU assays and semi-quantitative comparisons of Ki-67 mRNA expression. Both readouts pointed to a reduced proliferation in all three knockout clones compared with parental cells and ARF6 control clones. Average proliferation rates (percentages of cells showing proliferation) ranged higher than 67% in all four control cell lines (mean 69% [64 to 74] across all three control clones), but amounted to 52% in the single knockout clone, and below 47% in both double knockout clones (48% [39 to 57] across all three knockout clones) after 72 hours of culture (Fig. 4A). Differences of similar extent were observed for Ki-67 mRNA contents after 48 hours of culture (Fig. 5A). Average $2^{-\Delta Ct}$ values ranged between 0.09 to 0.11 in all four control cell lines (0.096 [0.082 to 0.111] across all three control clones), but amounted

effects of NAV2729 in all cell lines in (B) and (C). Results are expressed as changes in plug diameter during indicated periods, and as ratios between plug area and whole well area. Contraction of cells reduces the diameters of matrix plugs, so that lower gel/well area ratios reflect higher contraction and higher gel/well area ratios reflect lower contraction. Consequently, gel/well area ratios are shown using y axes with reverse direction to visualize higher and lower contractions. Shown are all single values together with means from five independent experiments for each setting. In (A), values of each knockout clone were compared with a cluster containing all 15 values of all three control clones together by one-way ANOVA with Dunnett's tests (* $P < 0.05$, ** $P < 0.01$, *** $P < 0.001$ versus a control group composed of all values of A3, C6, and D7). Parental WPMY-1 cells were not included to statistical analyses. In (B) and (C), values from both groups were compared by two-tailed Student's t test in each diagram (* $P < 0.05$, ** $P < 0.01$, *** $P < 0.001$ versus DMSO).

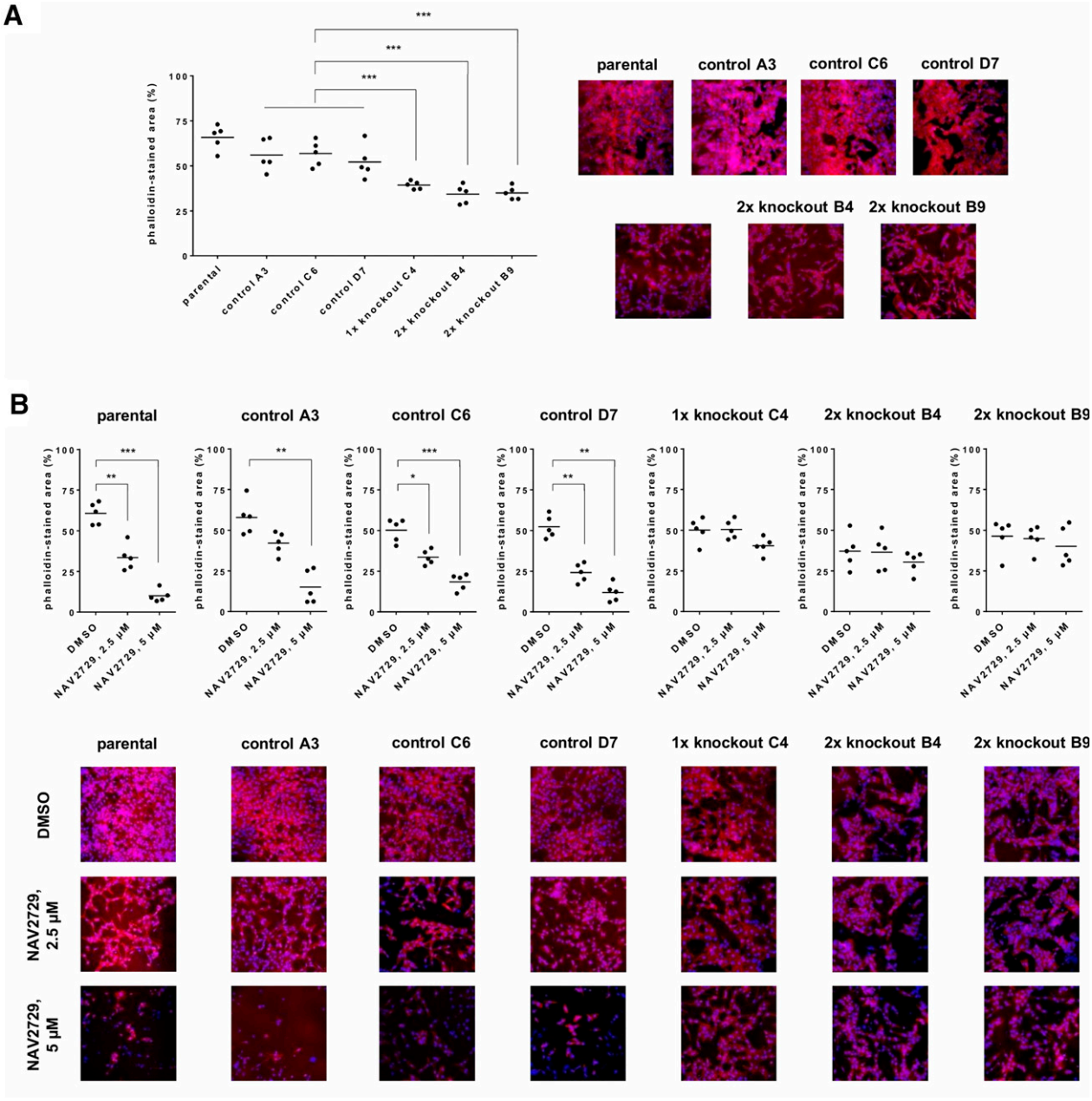

Fig. 3. Actin organization in WPMY1 cells, ARF6 control clones, and ARF6 knockout clones. Phalloidin staining was performed after cells were cultured for 72 hours without (A), or for 24 hours with (B) DMSO or NAV2729 in indicated concentrations. Subsequently, actin polymers were stained by phalloidin, resulting in red staining of polymerized actin. Nuclei were counterstained with DAPI (blue). Separate series of experiments were performed to compare actin organization between cell lines in (A), and to assess effects of NAV2729 in all cell lines in (B). Shown are all single values together with means from quantification of phalloidin-stained actin in five independent experiments for each setting together with representative images for each setting. In (A), values of each knockout clone were compared with a cluster containing all 15 values of all three control clones together by one-way ANOVA with Dunnett's tests (*** $P < 0.001$ versus a control group composed of all values of A3, C6, and D7). Parental WPMY-1 cells were not included to statistical analyses. In (B), values of each NAV2729 group were compared by one-way ANOVA with Dunnett's tests to values of the corresponding DMSO group (* $P < 0.05$, ** $P < 0.01$, *** $P < 0.001$ versus DMSO).

to 0.07 in the single knockout clone and ranged around 0.06 in both double knockout clones (0.065 [0.042 to 0.089] across all three knockout clones) (Fig. 5A).

In parental cells and ARF6 control clones, application of NAV2729 (2.5 µM, 5 µM) for 48 hours caused concentration-dependent inhibition of proliferation, resulting in virtually complete termination of proliferation activity by 5 µM NAV2729 in EdU assays (Fig. 4B). Across all three ARF6-expressing control clones, average percentages of proliferating cells ranged around 55% [39 to 71] after application of DMSO, but around 44% [41 to 47] after application of 2.5 µM NAV2729 and around 1.4% [−0.2 to 2.9] after application of 5 µM NAV2729 (Fig. 4B). In ARF6 knockout clones, application of NAV2729 (2.5 µM, 5 µM) for 48 hours was without any effect on proliferation rates, apart from a small decrease after application of 5 µM to clones B4 (Fig. 4B). Across all three ARF6 knockout clones, average percentages of proliferating cells ranged around 47% [42 to 53] after application of DMSO,

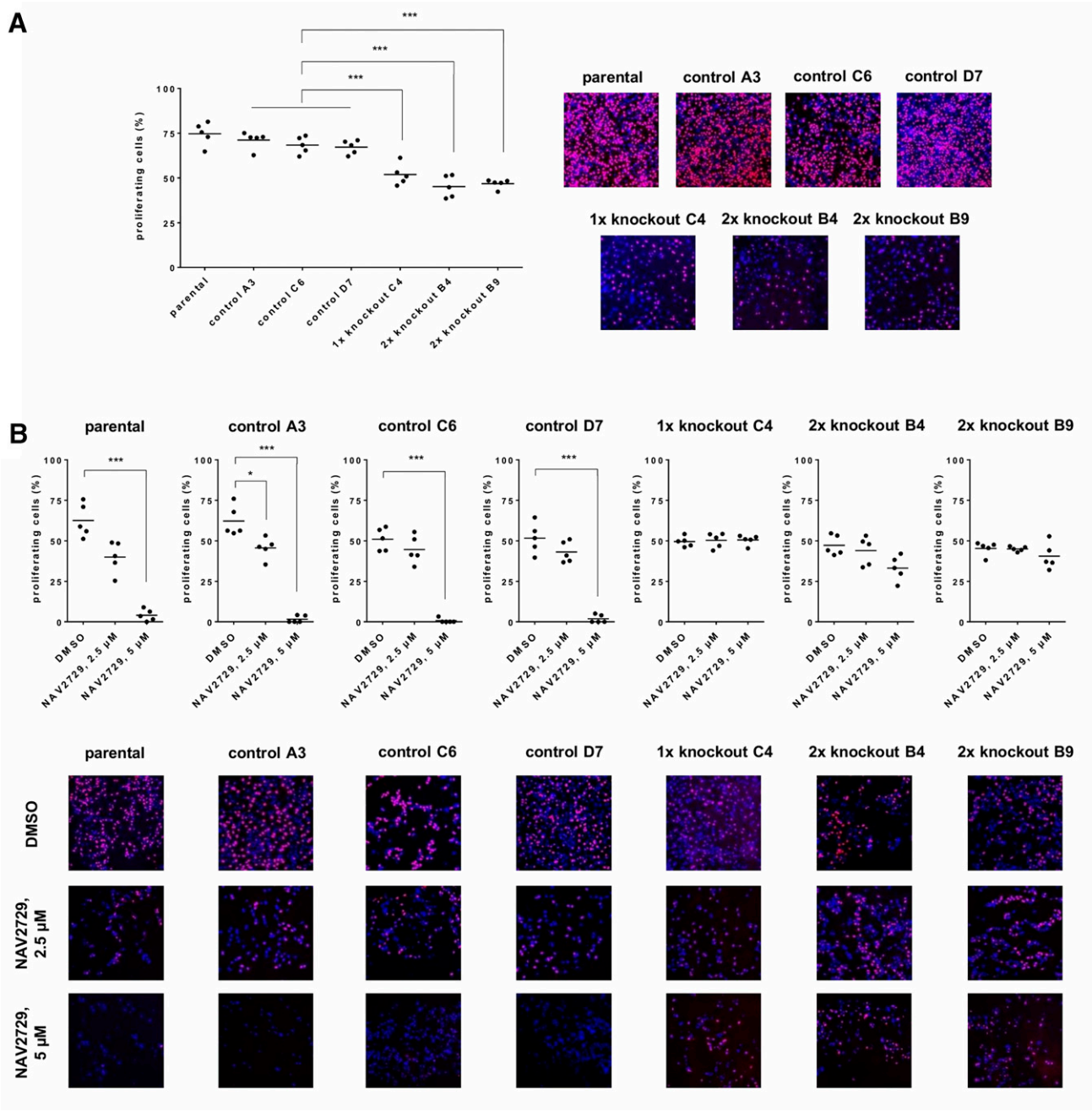

Fig. 4. Proliferation in WPMY1 cells, ARF6 control clones, and ARF6 knockout clones. Proliferation was assessed by EdU assays (red, proliferating cells; blue, nonproliferating cells) after cells were cultured for 72 hours without (A), or for 48 hours with (B) DMSO or NAV2729 in indicated concentrations. Separate series of experiments were performed to compare proliferation between cell lines in (A), and to assess effects of NAV2729 in all cell lines in (B). Shown are all single values together with means from quantification of proliferating cells in five independent experiments together with representative images for each setting. In (A), values of each knockout clone were compared with a cluster containing all 15 values of all three control clones together by one-way ANOVA with Dunnett's tests (*** $P < 0.001$ versus a control group composed of all values of A3, C6, and D7). Parental WPMY-1 cells were not included to statistical analyses. In (B), values of each NAV2729 group were compared by one-way ANOVA with Dunnett's tests to values of the corresponding DMSO group (* $P < 0.05$, ** $P < 0.01$, *** $P < 0.001$ versus DMSO).

around 46% [38 to 55] after application of 2.5 µM NAV2729, and around 41% [20 to 63] after application of 5 µM NAV2729 (Fig. 4B).

Effects of 5 µM NAV2729 on proliferation were confirmed by assessment of Ki-67 mRNA content (Fig. 5B). 5 µM NAV2729 reduced the content of Ki-67 mRNA in all cell lines, which was clearer and stronger in ARF6-expressing control cell lines compared with knockout clones (Fig. 5B). Thus, after application of 5 µM NAV2729, relative $2^{-\Delta Ct}$ values ranged around 0.34-fold of corresponding DMSO controls [0.25 to 0.43] across all three ARF6-expressing control clones, but around 0.73-fold of corresponding DMSO controls [0.68 to 0.77] across all three ARF6 knockout clones (Fig. 5B).

Effects of NAV2729 and ARF6 Knockout on Apoptosis and Cell Death. Numbers of apoptotic and dead cells were assessed by flowcytometry using labeling for 7-AAD and

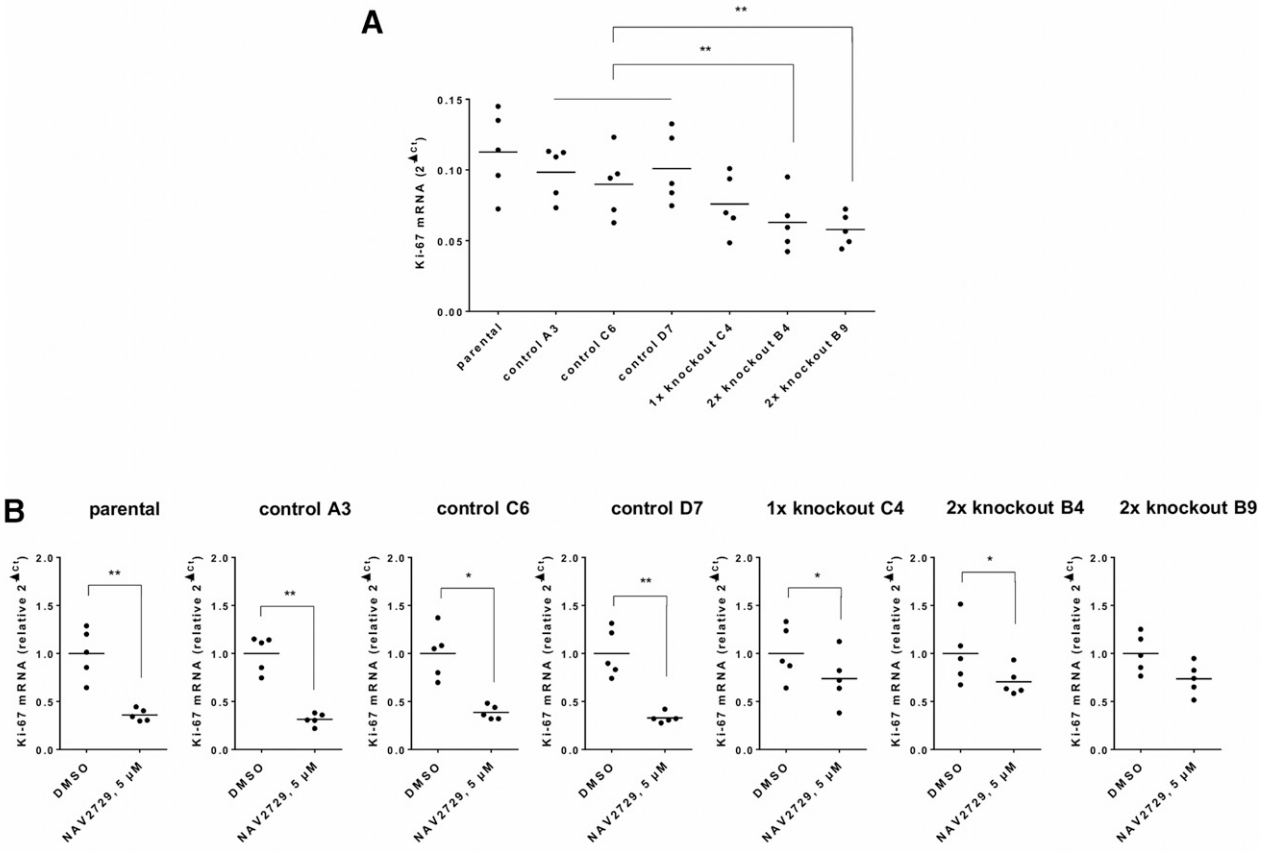

Fig. 5. Ki-67 mRNA content in WPMY1 cells, ARF6 control clones, and ARF6 knockout clones. Ki-67 mRNA content was assessed by RT-PCR, after cells were cultured for 24 hours with DMSO in required amounts, or NAV2729 in indicated concentrations. Data in (A) and (B) are derived from the same experiments, and include $2^{-\Delta Ct}$ values for comparison of Ki-67 content between the different cell lines in (A) and $2^{-\Delta Ct}$ values normalized to the mean of the corresponding DMSO group to assess the effects of NAV2729 in each cell line in (B). Shown are all single values together with means from five independent experiments. In (A), values of each knockout clone were compared with a cluster containing all 15 values of all three control clones together by one-way ANOVA with Dunnett's tests (** $P < 0.01$, *** $P < 0.001$ versus a control group composed of all values of A3, C6, and D7). Parental WPMY-1 cells were not included to statistical analyses. In (B), values from both groups were compared by two-tailed Student's t test in each diagram (* $P < 0.05$, ** $P < 0.01$, *** $P < 0.001$ versus DMSO).

annexin V. Compared with parental cells and ARF6 control clones, the percentage of apoptotic cells (annexin V–positive, 7-AAD–negative) and the percentage of dead cells (annexin V–positive, 7-AAD–positive, resulting either from apoptosis or necrosis) were increased in all three knockout clones after 48 hours of culture. Although the average percentage of apoptotic cells did not exceed 5% in control cell lines (mean 3.8% [1.7 to 5.9] across all three control clones), it exceeded 18% in all three knockout clones (20.4% [11.4 to 29.4] across all three knockout clones) (Fig. 6A). Similarly, the percentage of dead cells ranged below 6% in all three control cell lines (4.5% [2.7 to 6.3] across all three control clones), but above 15% in all three knockout clones (17.4% [13.3 to 21.6] across all three control clones) (Fig. 6A).

Similar rates were observed in cells treated with DMSO, as controls for NAV2729 (Fig. 6B). Application of NAV2729 (5 μM) for 24 hours increased the percentages of apoptotic and dead cells in all four control cell lines with ARF6 expression, but not in ARF6 knockout clones (Fig. 6B). Thus, across all three ARF6-expressing control clones, the average percentage of apoptotic cells ranged around 3% [1.4 to 4.8] after treatment with DMSO, but around 15% [13 to 17] after treatment with NAV2729 (Fig. 6B). Across all three ARF6 knockout clones, the average percentage of apoptotic cells ranged around 22% [−10 to 54] after treatment with DMSO, and around 19% [−20 to 58] after treatment with NAV2729 (Fig. 6B). Similarly, and across all three ARF6-expressing control clones, the average percentage of dead cells ranged around 5% [1.5 to 8.7] after treatment with DMSO, but around 31% [17 to 46] after treatment with NAV2729 (Fig. 6B). Across all three ARF6 knockout clones, the average percentage of dead cells ranged around 21% [9 to 33] after treatment with DMSO, and around 25% [16 to 35] after treatment with NAV2729 (Fig. 6B).

Effects of NAV2729 and ARF6 Knockout on Viability. Viability of cells was assessed by CCK-8 assays, and increased with culture time (48–96 hours), at least in ARF6-expressing control cell lines (Fig. 7A). The viability was lower in all three ARF6 knockout clones compared with parental cells and ARF6 control clones, what was best obvious after 72 hours and 96 hours of culture (Fig. 7A). Across all three ARF6-expressing control clones, average OD values ranged around 0.78 [0.76 to 0.80], but around 0.46 [0.21 to 0.70] across all three knockout clones after 72 hours of culture. After 96 hours of culture, average ratios between OD values ranged around 1.35 [1.32 to 1.39] across all three control clones, but around 0.51 [0.06 to 0.96] across all three knockout clones.

In cells with ARF6 expression, application of NAV2729 (24 hours) caused concentration-dependent decreases in viability,

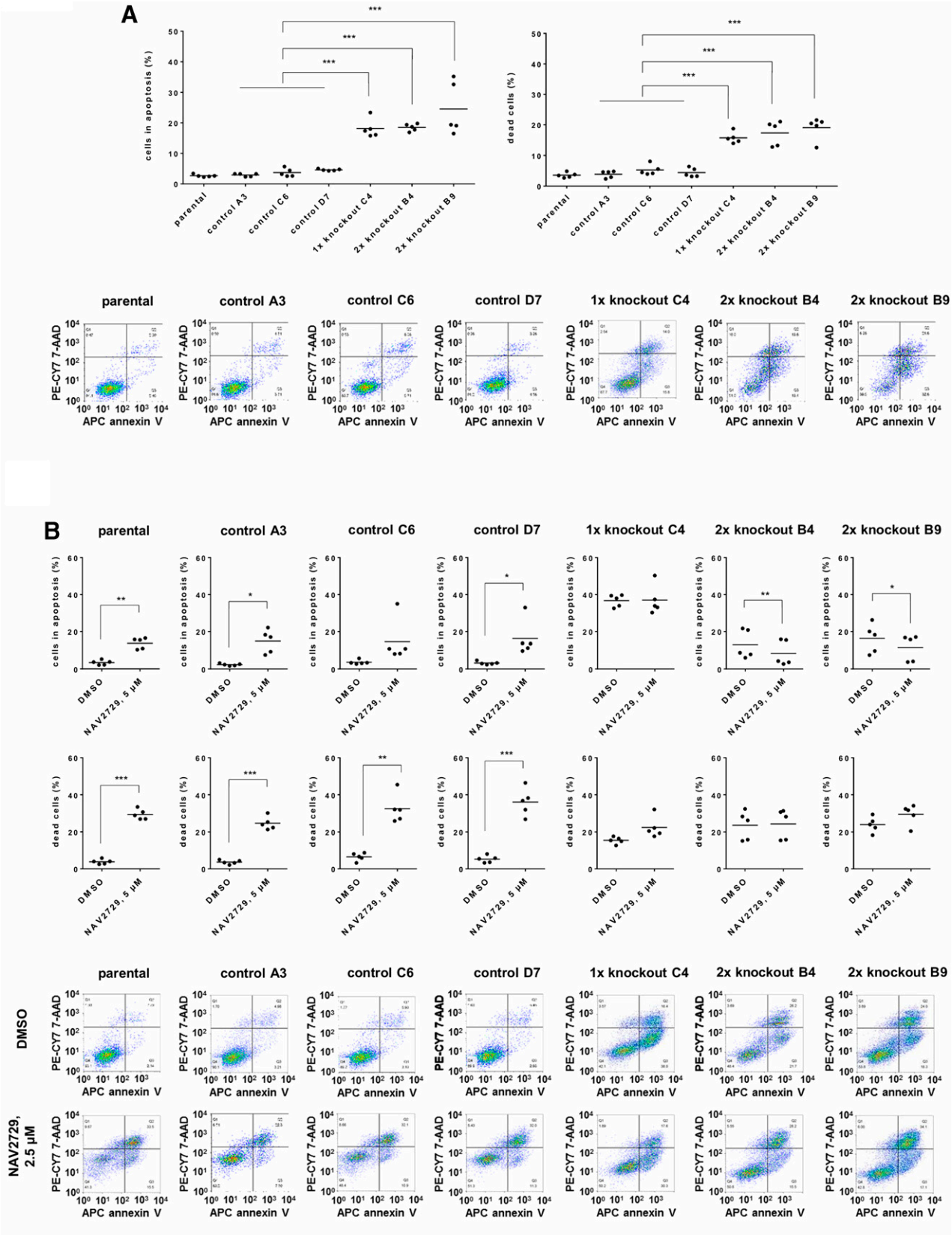

Fig. 6. Apoptosis and cell death in WPMY1 cells, ARF6 control clones, and ARF6 knockout clones. Flow cytometry was performed after cells were cultured for 48 hours without (A), or for 24 hours with (B) DMSO or NAV2729 in indicated concentrations. Subsequently, numbers of cells being in apoptosis (annexin V–positive, phycoerythrin/cyanine (PE-CY)7-AAD–negative) and of dead cells (resulting from apoptosis and/or necrosis; annexin V–positive, 7-AAD–positive) were assessed by flow cytometry. Separate series of experiments were performed to compare apoptosis and cell death between cell lines in (A) and to assess effects of NAV2729 in all cell lines in (B). Shown are all single values together with means from quantification of five independent experiments and representative experiments for each setting. In (A), values of each knockout clone were

with similar patterns in WPMY-1 cells and all three monoclonal ARF6 control clones. Thus, decreases in viability were observed using all concentrations (1 μM–6.5 μM), starting with moderate or slight decreases at 1 μM, whereas 6.5 μM nearly completely reduced viability (Fig. 7B). Across all three ARF6-expressing control clones and compared with the corresponding DMSO-treated controls, 1 μM reduced the OD values by 26% [7 to 44], 2.5 μM by 45% [19 to 70], 5 μM by 82% [71 to 93], and 6.5 μM by 91% [86 to 97] (Fig. 7B). Across all three ARF6 knockout clones and compared with the corresponding DMSO-treated controls, 1 μM reduced the OD values by 1.8% [−26 to 29], 2.5 μM by 11% [−24 to 45], 5 μM by 50% [−2 to 101], and 6.5 μM by 77% [43 to 111] (Fig. 7B).

Considering the concentration-dependent effects in these experiments, calculation of IC_{50} values for NAV2729 appeared in principle possible, but was limited by the uncertainty whether maximum effects were attained in the applied concentration range. To calculate IC_{50} values for NAV2729, effects on viability were assessed using a broader concentration range from 1.25 μM to 15 μM (Fig. 7C). In this range, NAV2729 completely inhibited viability in all cell lines (Fig. 7C). Calculation of IC_{50} values by curve fitting pointed to increased IC_{50} values for NAV2729 in ARF6-expressing cell lines compared with knockout clones. Thus, IC_{50} values amounted to 3.2 μM [2.8 to 3.5] in parental WPMY-1 cells, 3.3 μM [3 to 3.6] in control clone A3, 3.7 μM [2.6 to 4.8] in control clone C6, and 3.0 μM [2.4 to 3.6] in control clone D7, but to 8.2 μM [7.4 to 9] in knockout clone C4, 4.5 μM [4.1 to 4.9] in knockout clone B4, and 5 μM [4.2 to 5.7] in knockout clone B9 (Fig. 7C).

Discussion

Our findings point to a role of ARF6 in promotion of contraction and proliferation and in suppression of apoptosis in prostate stromal cells, and suggest a high specificity of the presumed ARF6 inhibitor NAV2729 within defined concentration ranges. To the best of our knowledge, this is the first evidence supporting a role of ARF6 in smooth muscle contraction using a knockout model. ARF6-mediated proliferation and suppression of apoptosis may both be involved in stromal growth and hyperplasia. In BPH, prostate smooth muscle contraction and stromal growth contribute to LUTS. Combination therapies are commonly applied to address contraction and growth at once in BPH. Here, both were targeted by NAV2729 in vitro. As other, established mediators of smooth muscle contraction are shared by different types of smooth muscle, investigation of similar ARF6 functions in other smooth muscle-rich organs merits further attention.

Compared with ARF6-expressing control clones, ARF knockout clones showed reduced contractions, impaired actin organization, decreased proliferation, increased apoptosis and cell death, and reduced overall survival. The possibly strongest of these changes were the increases in apoptosis and cell death. Previous evidence for ARF6-mediated suppression of apoptosis and cell death is limited, but available from prostate cancer cells, T cells, glioblastoma and osteosarcoma cells, and *Caenorhabditis elegans*, and included suppression of apoptosis and nonapoptotic cell death by ARF6 (Bhanot et al., 2010; Kutscher et al., 2018; Lei et al., 2020; Sumiyoshi et al., 2021). Cell death in annexin V–positive/7-AAD–positive cells detected in our flowcytometry analyses may result either from apoptosis or necrosis. Assuming that the difference between dead (annexin V–positive/7-AAD–positive) and apoptotic cells (annexin V–positive/7-AAD–negative) may mostly represent necrosis, our findings may suggest that cell death in knockout clones was predominantly or nearly exclusively caused by apoptosis, and that the contribution of necrosis may have been small or even neglectable. In fact, the results from all three knockouts are very similar and may confirm each other to this regard. After application of NAV2729 to control clones, the number of dead cells exceeded the number of apoptotic cells (roughly 2-fold), so that necrosis may have been involved in NAV2729 effects in control clones. This divergence between ARF6 knockout clones and NAV2729-treated control clones can be hardly interpreted without speculations. In contrast to some other series, where different concentrations of NAV2729 were applied, NAV2729 was applied only at a single concentration (5 μM) in our flowcytometry experiments, what may limit comparisons between untreated knockout clones and NAV2729-treated control clones. Focusing on the definitive conclusions, we observed that 1) ARF6 knockout strongly increased cell death and apoptosis, both parameters to similar degree, 2) that NAV2729 increased both in control clones, but 3) not at all in knockout clones.

In parallel to increased apoptosis, ARF6 knockout resulted in a reduced proliferation rate and in reduced mRNA expression of the proliferation marker Ki-67. ARF6-mediated proliferation has been documented for several cell types, including cancer cells and vascular smooth muscle cells (Li et al., 2017; Charles et al., 2018; Bourmoum et al., 2016). Our current findings from ARF6 knockout clones confirm our previous findings that silencing of ARF6 expression by transfection with siRNA reduced proliferation of WPMY-1 cells (Yu et al., 2019). ARF6 may drive survival of prostate stromal cells by dual contributions of ARF6-mediated proliferation and ARF6-mediated suppression of apoptosis, finally resulting in the reduced viability of knockout clones observed in viability assays. Together, it appears possible that ARF6 promotes stromal growth or prostate enlargement in BPH. In fact, BPH includes stromal hyperplasia, which may contribute to prostatic enlargement alone or together with epithelial hyperplasia (Strand et al., 2017).

ARF6 knockout clones showed reduced contractions in contractility assays, indicating a procontractile function of ARF6 in our cells. The parental cell line (i.e., WPMY-1 cells) were derived from the prostate stroma where smooth muscle cells are the predominant cell type. WPMY-1 cells show characteristics of prostate smooth muscle cells, including expression of α-smooth muscle actin, calponin, and α_{1A}-adrenoceptors, whereas markers characteristic for epithelial, glandular cells are not detectable (Webber et al., 1999; Wang et al., 2015, 2016). Reduced contractions in knockout clones were paralleled by impaired actin organization. The latter may well account for reduced contractions in knockouts, as it is critical

compared with a cluster containing all 15 values of all three control clones together by one-way ANOVA with Dunnett's tests (*** $P < 0.001$ versus a control group composed of all values of A3, C6, and D7). Parental WPMY-1 cells were not included to statistical analyses. In (B), values from both groups were compared by two-tailed Student's t test in each diagram (* $P < 0.05$, ** $P < 0.01$, *** $P < 0.001$ versus DMSO).

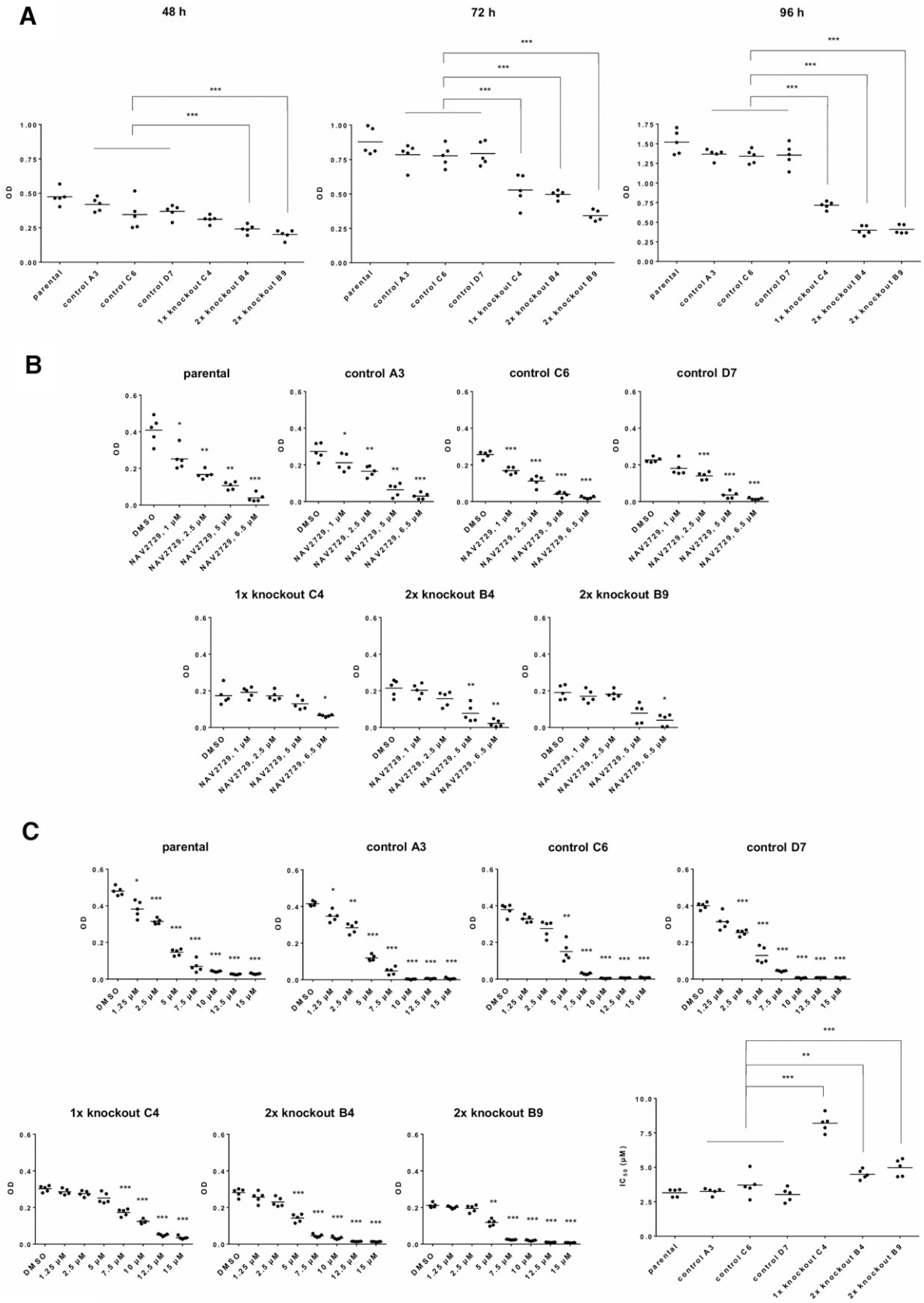

Fig. 7. Viability of WPMY1 cells, control clones, and ARF6 knockout clones, and IC_{50} values for NAV2729. Cells were cultured for indicated periods without (A), or for 24 hours with (B and C) DMSO or NAV2729 in indicated concentrations before viability was assessed by CCK-8 assay. Based on experiments shown in (C), IC_{50} values for NAV2729 were calculated for each cell line (C). Separate series of experiments were performed to compare viability between cell lines in (A), and to assess effects of NAV2729 in all cell lines in (B and C). Shown are all single values together with means from quantification of five independent experiments for each setting. In (A) and for comparison of IC_{50} values between

for contraction of any type of smooth muscle (Puetz et al., 2009; Hennenberg et al., 2014). Actin organization has been proposed as a major function of ARF6 (Schafer et al., 2000; Donaldson, 2002; Luton, 2005; Klein et al., 2006; Humphreys et al., 2013). In fact, other actin-dependent processes are susceptible to ARF6 inhibition or silencing as well, including migration of vascular smooth muscle cells (Charles et al., 2016, 2018, 2019).

A role of ARF6 in prostate smooth muscle contraction is in line with analog functions of other monomeric GTPases in smooth muscle contraction, which are emerging or already well established (Li et al., 2020b). RhoA-mediated smooth muscle contraction is widely accepted and proven for probably any smooth muscle type (Somlyo and Somlyo, 2003). More recently, similar roles in smooth muscle contraction have been proposed for other monomeric GTPases (Li et al., 2020b). In particular for Rac GTPases, a role in smooth muscle contraction in different organs becomes increasingly obvious (Li et al., 2020b). Other nonRhoA GTPases with supposed roles in regulation of smooth muscle contraction include rat sarcoma virus guanosine-5′-triphosphate hydrolyzing enzymes (RasGTPases), Ras-related protein Rap-1b (Rap1b), Ras-related protein Rab-11A (Rab11A), Ras-related protein Rab-35 (Rab35), and cell division protein 42 homolog (Cdc42) (Li et al., 2020b). It may be speculated that promotion of smooth muscle contraction by ARF6 is not limited to prostate smooth muscle but may occur in other smooth muscle-rich organs as well. Considering the high clinical relevance of smooth muscle contraction for pathophysiology and medical treatment of widespread diseases, investigation of ARF6 or NAV2729 in vascular, airway, and other smooth muscles appears reasonable.

In previous studies, NAV2729 showed IC_{50} values of 1 μM and 3.4 μM for ARF6 inhibition in fluorometric and orthogonal radiometric nucleotide exchange assays, but did not inhibit other ARF family members or other GTPases (Yoo et al., 2016). Calculation of IC_{50} values from our experiments addressing effects of NAV2729 on viability point to IC_{50} values between 3 and 3.7 μM in ARF6-expressing control cell lines, which were increased to 4.5–8.2 μM in knockout clones. Similarly, IC_{50} values around 2–3 μM may be estimated from our experiments based on phalloidin staining and EdU assays in ARF6-expressing cell lines, whereas effects by 5 μM NAV2729 were completely or nearly abolished in knockout cells in these experiments. In previous studies, a high degree of specificity for ARF6 has been proposed for NAV2729. Thus, NAV2729 was presumed to act with high specificity and selectivity of ARF6 even at concentrations of 50 μM, as neither RhoA, Ras-related C3 botulinum toxin substrate 1 (Rac1), H-Ras, Cdc42, or other ARF family members were inhibited in nucleotide exchange assays (Yoo et al., 2016). Application of 5 μM NAV2729 to WPMY-1 cells in our previous study inhibited ARF6, but not ARF1, Rac1, or RhoA (Yu et al., 2019). On the other hand, the specificity for ARF6 was challenged by a study reporting inhibition of ARF1 by 25 μM NAV2729 in nucleotide exchange assays, by inhibition of an ARF-GEF (Benabdi et al., 2017). However, effects of 5 μM NAV2729 in prostate tissues were not mimicked by the ARF1 inhibitor brefeldin A, so that ARF1 inhibition does not occur or is not relevant at concentrations up to 5 μM in prostate cells (Benabdi et al., 2017). In some series with knockout clones, we observed small effects using 5 μM to 15 μM NAV2729, what may reflect off-target effects at concentrations ≥5 μM, but may be explained by inhibition of remaining ARF6 as well.

As we observed that NAV2729 showed strong effects using concentrations up to 5 μM in ARF6-expressing cells, which were widely lacking in ARF6 knockout clones, we assume that NAV2729 acts mostly without off-target effects and ARF6-specific at concentrations up to 5 μM in our cells. In ARF6-expressing clones, 5 μM and lower concentrations showed large effects on contractility, actin organization, proliferation, apoptosis and cell death, and viability. In contrast, no or only small effects were observed using the same concentrations in knockout clones. Concentrations below 5 μM showed clear effects in some experiments with ARF6-expressing cells, which were completely blunted in knockout cells. Consequently, NAV2729 is obviously specific for ARF6, at least at concentrations up to 5 μM in our cells. Apparently, NAV2729 inhibits proliferation, survival, and contraction, and increases apoptosis and cell death in prostate stromal by specific inhibition of ARF6, whereas contributions from off-target inhibition to these effects may be neglectable or lacking. Taking this specificity into account, it appears likely that the recently described inhibition of prostate smooth muscle contraction in human tissues by 5 μM NAV2729 was in fact caused by inhibition of ARF6 (Yu et al., 2019). Previous evidence suggesting inhibition of proliferation by NAV2729 in any cell type is surprisingly rare, if not limited to our previous findings obtained with WPMY-1 cells (Yu et al., 2019).

Overall, the effect of ARF6 knockout was remarkably similar between knockout at one allele compared with knockouts at two alleles. Generally, it is aimed to knockout all alleles in a cell to obtain complete and clean knockout. Although our clones were monoclonized by two consecutive single cell dilutions and monoclonality was assured, all clones still showed three alleles in the MiSeq analysis. The results indicate that the cell line itself is not diploid, but triploid, in line with previous characterization of the parental cell line (Webber et al., 1999). Impurities or insufficient sequencing in the MiSeq analysis can be excluded as two independent rounds of sequencing showed the same output. In fact, we expected a stronger knockout phenotype in clones where two out of three alleles were knocked out compared with those where only one out of three alleles was knocked out. The lacking functional difference between one or two out of three knocked out alleles may indicate that already interrupting the Arf6 sequence in one allele is sufficient to lower the ARF6 protein expression drastically and that the remaining intact alleles are not sufficient to compensate the missing one. Another possibility could be off-target effects from the guideRNA. Although there was no indel detected at the site of editing for the gray pie chart alleles, successful ARF6 protein expression could be impaired by off-target effects from the guideRNA in

clones, values of each knockout clone were compared with a cluster containing all 15 values of all three control clones together by one-way ANOVA with Dunnett's tests (** $P < 0.01$, *** $P < 0.001$ versus a control group composed of all values of A3, C6, and D7). Parental WPMY-1 cells were not included to statistical analyses. In (B) and (C) (except comparison of IC_{50} values), values of each NAV2729 group were compared by one-way ANOVA with Dunnett's tests to values of the corresponding DMSO group (* $P < 0.05$, ** $P < 0.01$, *** $P < 0.001$ versus DMSO).

regions close or in the Arf6 sequence, but outside the detection frame from the MiSeq analysis.

Together, our findings suggest a dual role of ARF6 for smooth muscle contraction and stromal growth in the prostate. Identifying the involved molecular mechanisms merits further attention by future studies. Smooth muscle contraction and stromal growth can both contribute to urethral obstruction in BPH, resulting in impaired bladder emptying and voiding, and finally in LUTS suggestive of BPH (Hennenberg et al., 2014). Accordingly, both factors are important targets for medical therapy (Oelke et al., 2013; Hennenberg et al., 2014). Combination therapies are applied to address both processes at once (Fullhase et al., 2013; Oelke et al., 2013). For decades, smooth muscle contraction and growth in BPH were mostly considered separately. Obviously, both are not independent players in driving LUTS, as previously assumed, but rather linked with each other by ARF6. Similar connections between contraction and proliferation are well evidenced in other context, with RhoA/Rho kinase mediating both process in vascular smooth muscle probably as one of the best examples (Shimokawa et al., 2016).

For treatment of voiding symptoms, α_1-adrenoceptor antagonists and the phosphodiesterase-5 inhibitor tadalafil are available (Oelke et al., 2013). Both may improve maximum urinary flow rate and symptom scores by relaxation of prostate smooth muscle (Oelke et al., 2013). For prevention of progression and complications, 5α-reductase inhibitors are applied, which may reduce prostate size by inhibition of testosterone-dependent growth (Oelke et al., 2013). However, improvements of symptoms and urinary flow rate are limited to 40%–50%, whereas even placebos may show improvements around 30%, and the percentage of nonresponders amounts up to 30%–35% (Kortmann et al., 2003; Madersbacher et al., 2007; Chapple et al., 2011; Eredics et al., 2017). Combination therapies are, in turn, characterized by low tolerability, and show no additive benefits regarding the improvements of symptoms and urinary flow (Fullhase et al., 2013). Consequently, discontinuation due to unbalanced side effects and disappointing efficacy is common, amounting up to 65% within one year even for monotherapy with α_1-adrenoceptor antagonists, and accounting for progression, complications, hospitalization, and surgery for BPH (Cindolo et al., 2015a, 2015b). Thus, novel medications may be appreciated, and identification of molecular mechanisms with dual functions in contraction and growth in BPH may offer novel perspectives to develop single compounds targeting both at once. At least in vitro, both processes were inhibited by NAV2729 in our study, demonstrating that such compounds are in principle available.

ARF6 promotes smooth muscle contraction and proliferation in the human prostate stroma. Both can be inhibited by NAV2729, which acts without off-target effect up to 5 μM in prostate stromal role. ARF6 merits further investigation in the context of smooth muscle contraction in other smooth muscle-rich organs.

Acknowledgments

We thank Dr. Veit Hornung and Stefan Bauernfried (Gene Center and Department of Biochemistry, LMU Munich, Munich, Germany) for providing us plasmids, and their support with separation of transfected cells and sequencing. We thank Dr. Elfriede Noessner and her coworkers (Institute of Molecular Immunology, Helmholtz Center, Munich) for their support with immunofluorescence microscopy.

Authorship Contributions

Participated in research design: Wang, Keppler, Stief, Hennenberg.

Conducted experiments: Wang, Schneider, Li, Rutz, Ciotkowska, Hennenberg.

Performed data analysis: Wang, Schneider, Li, Rutz, Ciotkowska, Hennenberg.

Wrote or contributed to the writing of the manuscript: Wang, Schneider, Keppler, Stief, Hennenberg.

References

Benabdi S, Peurois F, Nawrotek A, Chikireddy J, Cañeque T, Yamori T, Shiina I, Ohashi Y, Dan S, Rodriguez R, et al. (2017) Family-wide analysis of the inhibition of Arf guanine nucleotide exchange factors with small molecules: evidence of unique inhibitory profiles. *Biochemistry* **56**:5125–5133.

Bhanot H, Young AM, Overmeyer JH, and Maltese WA (2010) Induction of nonapoptotic cell death by activated Ras requires inverse regulation of Rac1 and Arf6. *Mol Cancer Res* **8**:1358–1374.

Bourmoum M, Charles R, and Claing A (2016) The GTPase ARF6 controls ROS production to mediate angiotensin II-induced vascular smooth muscle cell proliferation. *PLoS One* **11**:e0148097.

Chapple CR, Montorsi F, Tammela TL, Wirth M, Koldewijn E, and Fernández Fernández E; European Silodosin Study Group (2011) Silodosin therapy for lower urinary tract symptoms in men with suspected benign prostatic hyperplasia: results of an international, randomized, double-blind, placebo- and active-controlled clinical trial performed in Europe. *Eur Urol* **59**:342–352.

Charles R, Bourmoum M, Campbell S, and Claing A (2019) Methods to investigate the β-arrestin-mediated control of ARF6 activation to regulate trafficking and actin cytoskeleton remodeling. *Methods Mol Biol* **1957**:159–168.

Charles R, Bourmoum M, and Claing A (2018) ARF GTPases control phenotypic switching of vascular smooth muscle cells through the regulation of actin function and actin dependent gene expression. *Cell Signal* **46**:64–75.

Charles R, Namkung Y, Cotton M, Laporte SA, and Claing A (2016) β-arrestin-mediated angiotensin II signaling controls the activation of ARF6 protein and endocytosis in migration of vascular smooth muscle cells. *J Biol Chem* **291**: 3967–3981.

Choi WH, Kim J, Lee YR, Lee CK, Kim YS, Kim J, Choi YJ, Woo NS, Cho S, and Kim B (2005) Cdc42 contributes to phorbol ester-induced Ca2+-independent contraction of pulmonary artery smooth muscle. *J Vet Med Sci* **67**:787–793.

Cindolo L, Pirozzi L, Fanizza C, Romero M, Tubaro A, Autorino R, De Nunzio C, and Schips L (2015a) Drug adherence and clinical outcomes for patients under pharmacological therapy for lower urinary tract symptoms related to benign prostatic hyperplasia: population-based cohort study. *Eur Urol* **68**:418–425.

Cindolo L, Pirozzi L, Sountoulides P, Fanizza C, Romero M, Castellan P, Antonelli A, Simeone C, Tubaro A, de Nunzio C, et al. (2015b) Patient's adherence on pharmacological therapy for benign prostatic hyperplasia (BPH)-associated lower urinary tract symptoms (LUTS) is different: is combination therapy better than monotherapy? *BMC Urol* **15**:96.

D'Souza-Schorey C and Chavrier P (2006) ARF proteins: roles in membrane traffic and beyond. *Nat Rev Mol Cell Biol* **7**:347–358.

Dai F, Qi Y, Guan W, Meng G, Liu Z, Zhang T, and Yao W (2019) RhoGDI stability is regulated by SUMOylation and ubiquitination via the AT1 receptor and participates in Ang II-induced smooth muscle proliferation and vascular remodeling. *Atherosclerosis* **288**:124–136.

Donaldson JG (2002) Arf6 and its role in cytoskeletal modulation. *Methods Mol Biol* **189**:191–198.

Eredics K, Madersbacher S, and Schauer I (2017) A relevant midterm (12 months) placebo effect on lower urinary tract symptoms and maximum flow rate in male lower urinary tract symptom and benign prostatic hyperplasia-A meta-analysis. *Urology* **106**:160–166.

Füllhase C, Chapple C, Cornu JN, De Nunzio C, Gratzke C, Kaplan SA, Marberger M, Montorsi F, Novara G, Oelke M, et al. (2013) Systematic review of combination drug therapy for non-neurogenic male lower urinary tract symptoms. *Eur Urol* **64**:228–243.

Gauthier-Campbell C, Bredt DS, Murphy TH, and El-Husseini Ael-D (2004) Regulation of dendritic branching and filopodia formation in hippocampal neurons by specific acylated protein motifs. *Mol Biol Cell* **15**:2205–2217.

Halwani R, Vazquez-Tello A, Sumi Y, Pureza MA, Bahammam A, Al-Jahdali H, Soussi-Gounni A, Mahboub B, Al-Muhsen S, and Hamid Q (2013) Eosinophils induce airway smooth muscle cell proliferation. *J Clin Immunol* **33**:595–604.

Hennenberg M, Stief CG, and Gratzke C (2014) Prostatic α1-adrenoceptors: new concepts of function, regulation, and intracellular signaling. *Neurourol Urodyn* **33**:1074–1085.

Hiroi T, Someya A, Thompson W, Moss J, and Vaughan M (2006) GEP100/BRAG2: activator of ADP-ribosylation factor 6 for regulation of cell adhesion and actin cytoskeleton via E-cadherin and alpha-catenin. *Proc Natl Acad Sci USA* **103**:10672–10677.

Hongu T and Kanaho Y (2014) Activation machinery of the small GTPase Arf6. *Adv Biol Regul* **54**:59–66.

Hongu T, Yamauchi Y, Funakoshi Y, Katagiri N, Ohbayashi N, and Kanaho Y (2016) Pathological functions of the small GTPase Arf6 in cancer progression: Tumor angiogenesis and metastasis. *Small GTPases* **7**:47–53.

Humphreys D, Davidson AC, Hume PJ, Makin LE, and Koronakis V (2013) Arf6 coordinates actin assembly through the WAVE complex, a mechanism usurped by Salmonella to invade host cells. *Proc Natl Acad Sci USA* **110**:16880–16885.

Jones MC, Zha J and Humphries MJ (2019) Connections between the cell cycle, cell adhesion and the cytoskeleton. *Philos Trans R Soc Lond B Biol Sci* **374(1779)**: 20180227.

Klein S, Franco M, Chardin P, and Luton F (2006) Role of the Arf6 GDP/GTP cycle and Arf6 GTPase-activating proteins in actin remodeling and intracellular transport. *J Biol Chem* **281**:12352–12361.

Kortmann BB, Floratos DL, Kiemeney LA, Wijkstra H, and de la Rosette JJ (2003) Urodynamic effects of alpha-adrenoceptor blockers: a review of clinical trials. *Urology* **62**:1–9.

Kutscher LM, Keil W, and Shaham S (2018) RAB-35 and ARF-6 GTPases mediate engulfment and clearance following linker cell-type death. *Dev Cell* **47**:222–238.e6.

Lei H, Ma F, Jia R, and Tan B (2020) Effects of Arf6 downregulation on biological characteristics of human prostate cancer cells. *Int Braz J Urol* **46**:950–961.

Li B, Wang R, Wang Y, Stief CG, and Hennenberg M (2020a) Regulation of smooth muscle contraction by monomeric non-RhoA GTPases. *Br J Pharmacol* **177**: 3865–3877.

Li B, Wang R, Wang Y, Stief CG, and Hennenberg M (2020b) Regulation of smooth muscle contraction by monomeric non-RhoA GTPases. *Br J Pharmacol* **177**: 3865–3877.

Li R, Peng C, Zhang X, Wu Y, Pan S, and Xiao Y (2017) Roles of Arf6 in cancer cell invasion, metastasis and proliferation. *Life Sci* **182**:80–84.

Luton F (2005) The role of EFA6, exchange factor for Arf6, for tight junction assembly, functions, and interaction with the actin cytoskeleton. *Methods Enzymol* **404**:332–345.

Madersbacher S, Marszalek M, Lackner J, Berger P, and Schatzl G (2007) The long-term outcome of medical therapy for BPH. *Eur Urol* **51**:1522–1533.

Michel MC, Murphy TJ, and Motulsky HJ (2020) New author guidelines for displaying data and reporting data analysis and statistical methods in experimental biology. *Mol Pharmacol* **97**:49–60.

Miura Y, Hongu T, Yamauchi Y, Funakoshi Y, Katagiri N, Ohbayashi N, and Kanaho Y (2016) ACAP3 regulates neurite outgrowth through its GAP activity specific to Arf6 in mouse hippocampal neurons. *Biochem J* **473**:2591–2602.

Oelke M, Bachmann A, Descazeaud A, Emberton M, Gravas S, Michel MC, N'dow J, Nordling J, and de la Rosette JJ; European Association of Urology (2013) EAU guidelines on the treatment and follow-up of non-neurogenic male lower urinary tract symptoms including benign prostatic obstruction. *Eur Urol* **64**:118–140.

Puetz S, Lubomirov LT, and Pfitzer G (2009) Regulation of smooth muscle contraction by small GTPases. *Physiology (Bethesda)* **24**:342–356.

Schafer DA, D'Souza-Schorey C, and Cooper JA (2000) Actin assembly at membranes controlled by ARF6. *Traffic* **1**:892–903.

Schmid-Burgk JL, Schmidt T, Gaidt MM, Pelka K, Latz E, Ebert TS, and Hornung V (2014) OutKnocker: a web tool for rapid and simple genotyping of designer nuclease edited cell lines. *Genome Res* **24**:1719–1723.

Scholzen T and Gerdes J (2000) The Ki-67 protein: from the known and the unknown. *J Cell Physiol* **182**:311–322.

Schweitzer JK and D'Souza-Schorey C (2005) A requirement for ARF6 during the completion of cytokinesis. *Exp Cell Res* **311**:74–83.

Shimokawa H, Sunamura S, and Satoh K (2016) RhoA/Rho-Kinase in the cardiovascular system. *Circ Res* **118**:352–366.

Somlyo AP and Somlyo AV (2003) Ca2+ sensitivity of smooth muscle and nonmuscle myosin II: modulated by G proteins, kinases, and myosin phosphatase. *Physiol Rev* **83**:1325–1358.

Strand DW, Costa DN, Francis F, Ricke WA, and Roehrborn CG (2017) Targeting phenotypic heterogeneity in benign prostatic hyperplasia. *Differentiation* **96**:49–61.

Sumiyoshi M, Kotani Y, Ikuta Y, Suzue K, Ozawa M, Katakai T, Yamada T, Abe T, Bando K, Koyasu S, et al. (2021) Arf1 and Arf6 synergistically maintain survival of T cells during activation. *J Immunol* **206**:366–375.

Torii T, Miyamoto Y, Sanbe A, Nishimura K, Yamauchi J, and Tanoue A (2010) Cytohesin-2/ARNO, through its interaction with focal adhesion adaptor protein paxillin, regulates preadipocyte migration via the downstream activation of Arf6. *J Biol Chem* **285**:24270–24281.

Urban AE, Quick EO, Miller KP, Krcmery J, and Simon HG (2016) Pdlim7 regulates Arf6-dependent actin dynamics and is required for platelet-mediated thrombosis in mice. *PLoS One* **11**:e0164042.

Wang Y, Gratzke C, Tamalunas A, Wiemer N, Ciotkowska A, Rutz B, Waidelich R, Strittmatter F, Liu C, Stief CG, et al. (2016) P21-activated kinase inhibitors FRAX486 and IPA3: inhibition of prostate stromal cell growth and effects on smooth muscle contraction in the human prostate. *PLoS One* **11**:e0153312.

Wang Y, Kunit T, Ciotkowska A, Rutz B, Schreiber A, Strittmatter F, Waidelich R, Liu C, Stief CG, Gratzke C, et al. (2015) Inhibition of prostate smooth muscle contraction and prostate stromal cell growth by the inhibitors of Rac, NSC23766 and EHT1864. *Br J Pharmacol* **172**:2905–2917.

Webber MM, Trakul N, Thraves PS, Bello-DeOcampo D, Chu WW, Storto PD, Huard TK, Rhim JS, and Williams DE (1999) A human prostatic stromal myofibroblast cell line WPMY-1: a model for stromal-epithelial interactions in prostatic neoplasia. *Carcinogenesis* **20**:1185–1192.

Yamauchi Y, Miura Y, and Kanaho Y (2017) Machineries regulating the activity of the small GTPase Arf6 in cancer cells are potential targets for developing innovative anti-cancer drugs. *Adv Biol Regul* **63**:115–121.

Yoo JH, Shi DS, Grossmann AH, Sorensen LK, Tong Z, Mleynek TM, Rogers A, Zhu W, Richards JR, Winter JM, et al. (2016) ARF6 is an actionable node that orchestrates oncogenic GNAQ signaling in uveal melanoma. *Cancer Cell* **29**: 889–904.

Yu Q, Gratzke C, Wang R, Li B, Kuppermann P, Herlemann A, Tamalunas A, Wang Y, Rutz B, Ciotkowska A, et al. (2019) A NAV2729-sensitive mechanism promotes adrenergic smooth muscle contraction and growth of stromal cells in the human prostate. *J Biol Chem* **294**:12231–12249.

Address correspondence to: Dr. Martin Hennenberg, Urologische Klinik und Poliklinik, Marchioninistr. 15, 81377 München, Germany. E-mail: martin.hennenberg@med.uni-muenchen.de